nature chemistry

SUPPLEMENTARY INFORMATION

DOI: 10.1038/NCHEM.1432

Ab initio carbon capture in open-site metal–organic frameworks

Allison L. Dzubak,[¶,1] Li-Chiang Lin,[¶,2] Jihan Kim,[3] Joseph A. Swisher,[2,3] Roberta Poloni,[2,4] Sergey N. Maximoff,[2] Berend Smit,*[2,3] and Laura Gagliardi*[1]

[1]Department of Chemistry and Supercomputing Institute, University of Minnesota, 207 Pleasant Street SE, Minneapolis, Minnesota 55455-0431, USA

[2]Department of Chemical and Biomolecular Engineering and Chemistry, University of California, Berkeley, Berkeley, CA 94720-1462, USA

[3]Materials Science Division, Lawrence Berkeley National Laboratory, Berkeley, CA 94720, USA

[4]Molecular Foundry, Lawrence Berkeley National Laboratory, Berkeley, California

[¶] These authors contributed equally to this work
[*]Corresponding authors: Berend-Smit@berkeley.edu and gagliard@umn.edu

Contents

1. Detailed description of the MP2 calculations
    1.1 MP2 theory
    1.2 Description of the clusters
    1.3 Description of the charges
    1.4 Comparison between MP2 and vdW-DF
    1.5 Nemo decomposition
2. DFT calculations
    2.1 Details of the DFT calculations
    2.2 Crystal structure calculations
    2.3 CO_2-MOF interactions
3. Force field parameterization
4. Molecular simulations
    4.1 Force fields
    4.2 Simulation details
5. Study of extended Mg-MOF-74 (Mg_2(dobpdc))
    5.1 Description of the system
    5.2 CO_2 adsorption isotherms
6. Replacement of Mg with a different metal (Zn-MOF-74)
    6.1 Force field development
    6.2 Prediction of CO_2 adsorption properties
7. Extend to general structure (MOF-5)
    7.1 Description of the system
    7.2 Prediction of the CO_2 adsorption isotherm
8. Mixture isotherm predictions
9. Summary of force field parameters
10. Description of the difference clusters used in this study
11. Detailed acknowledgements

1 Detailed description of the MP2 calculations

1.1 MP2 theory

In this work, we have used second-order Møller-Plesset perturbation theory (MP2) to describe interactions of CO_2 and N_2 with MOFs. MP2 is adequate for the treatment of electron correlation in cases where strong correlations are not present.

In Mg-MOF-74, we have defined 8 representative clusters of the MOF to compute interactions with the guest, each cluster chosen to best represent the atom type to be parameterized (excluding H atom type). Within each cluster, the basis functions were chosen such that a larger contraction was used for the guest atoms, the atom type being approached in the MOF, and its nearest neighbors, while a smaller contraction was used for all atoms father away. The choice of clusters, basis function contractions, and discussion of convergence are given here. The interaction energies were determined by the supermolecular approach, counterpoise corrected for basis set superposition error.[1] All calculations have been performed using the MOLCAS[2] software version 7.6. Resolution of the identity (RI) and Cholesky decomposition (CD) techniques were employed to treat the two electron integrals.[3-5] The Douglas-Kroll Hess Hamiltonian[6] was used in conjunction with atomic natural orbital relativistic correlation consistent (ANO-RCC)[7,8] type of basis functions.

1.2 Description of the clusters

Atom types for the framework (Mg-MOF-74) were defined based on the symmetry of the periodic system, which has 9 distinct atom types. All metal sites are equivalent (Mg), each 2,5-dioxido-1, 4-benzenedicarboxylate (dobdc) linker has 3 types of oxygen atoms (O_a, O_b, O_c), 4 types of carbon atoms (C_a, C_b, C_c, C_d), and 1 type of hydrogen (H) shown in Figure SI 1. For each atom type (excluding H), a cluster was defined in a way to best represent the local environment of that atom type, shown in Figures SI 16-23 in section 10. Hydrogen was not explicitly considered for our parameterization due to its small contribution to the total interaction energy. The standard Universal force field[9] parameters for H were adapted to our functional form (all parameters are summarized in section 9).

The approaching path of the guest molecule was determined by the procedure described in section 3. The approaching paths of the guest (CO_2, N_2) to each MOF atom type are shown in Figures SI 16-23. For each path, separations *r* defined as the distance between the MOF atom type of interest and a) the nearest oxygen of CO_2 or b) the nearest nitrogen of N_2. At each of these points for each path, three MP2 calculations were performed to determine the interaction energy given by Equation (1), where the dummy functions are included as the CP correction for BSSE.[1] The ANO-RCC basis set contractions are given in captions of Figures SI 16-23.

$$E_{\text{int}} = E_{\text{MOF+guest}} - E_{\text{MOF+(dummy guest)}} - E_{\text{guest+(dummy MOF)}} \quad (1)$$

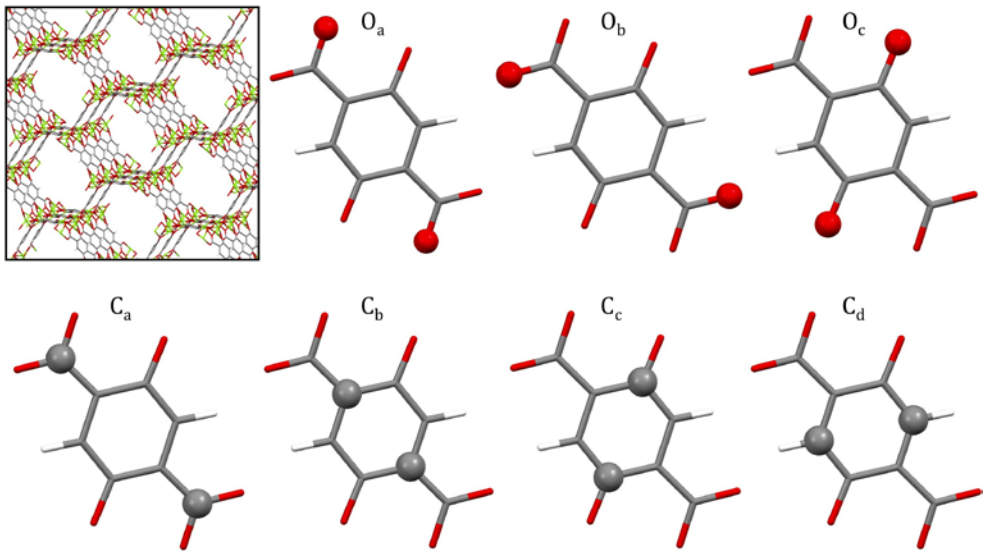

Figure SI 1: Image of Mg-MOF-74 structure (top left) where it is seen that all metal types are equivalent, and BDC linker atom types considered in our parameterization along with the naming scheme adopted here.

1.3 Description of the charges

The LoProp method[10] (based on MP2 densities[11]) was used to compute the localized electrostatic moments to second order and the dipole-dipole polarizabilities. This was done for each cluster, CO_2, and N_2. The choice of basis set contractions are identical to those used in computing the interaction energy. Output from this procedure provides for each atom: scalar charge, 3 components of dipole moment, 6 components of quadrupole moment, and 6 components of the polarizability. While only the interaction between point charges is used directly in the GCMC simulation, the other values contribute to the NEMO decomposition of the interaction energy (described in section 1.5).

It is important to note that these charges will be slightly different in each cluster due to the choice of truncation. Since the restriction is not imposed that each atom type has the same charge in the LoProp method (and that the symmetry of the various clusters is different than the symmetry of the periodic structure), the following was performed to assign the atom type charges for direct use in the GCMC simulations. For Mg-MOF-74, the charge for Mg atom type comes from the LoProp charge of the Mg being approached in the Mg cluster; this is not an average of the Mg charges since the local environment around the single Mg is best represented. The same was done for the 7 other atom type clusters, and H atom type was used to balance the overall charge such that the periodic structure remains neutral. All the charge parameters are given in section 9.

1.4 Comparison between MP2 and vdW-DF

The main disadvantage of MP2 calculations is that they are limited to a relatively small number of atoms. DFT would be more efficient to use for these systems, but conventional DFT does not include the van der Waals interactions. Recently, progress has been made

to include these in DFT (see section 2) and in this section we compare the MP2 results with the results obtained with a recently proposed van der Waals functional within DFT (vdw-DF).[13]

Figure SI 2 compares the energies of a CO_2 molecule approaching a cluster of Mg-MOF-74 calculated using MP2 and vdW-DF. Since DFT calculations use periodic boundary conditions, we employed a supercell large enough so that the interactions between the images could be ignored. The reported DFT energies include corrections for the basis set superposition errors. The results show an excellent agreement between the two methodologies. This is an important result as we can use the DFT calculations to test whether our MP2-derived force field can correctly predict the DFT data for the complete periodic MOF.

The agreement between the MP2 and DFT is also encouraging from a computational point of view as it suggests that a combination of the NEMO decomposition with DFT would allow us to use much larger systems. For the MOFs studied here, the ground state electron configurations can be described using a single slater determinant, so MP2 was used to obtain the reference properties *vide infra*. Higher levels of theory (such as coupled cluster) may also be used, however we did not find the additional computational expense necessary. For other MOF systems with open-shell metals (e.g., Fe), the MP2 description would not be adequate and the reference properties in the forthcoming studies of open-shell metals will be computed with a multi-determinental method (such as CASPT2).

The MP2 calculations in our manuscript typically take a few hours on a linux machine with 20 Gb of memory. To determine a force field we require of the order of 50-100 MP2 calculations. Once the force fields parameters have been determined a grand-canonical Monte Carlo simulation to compute the isotherms takes a few minutes on a GPU or a few hours on a CPU.

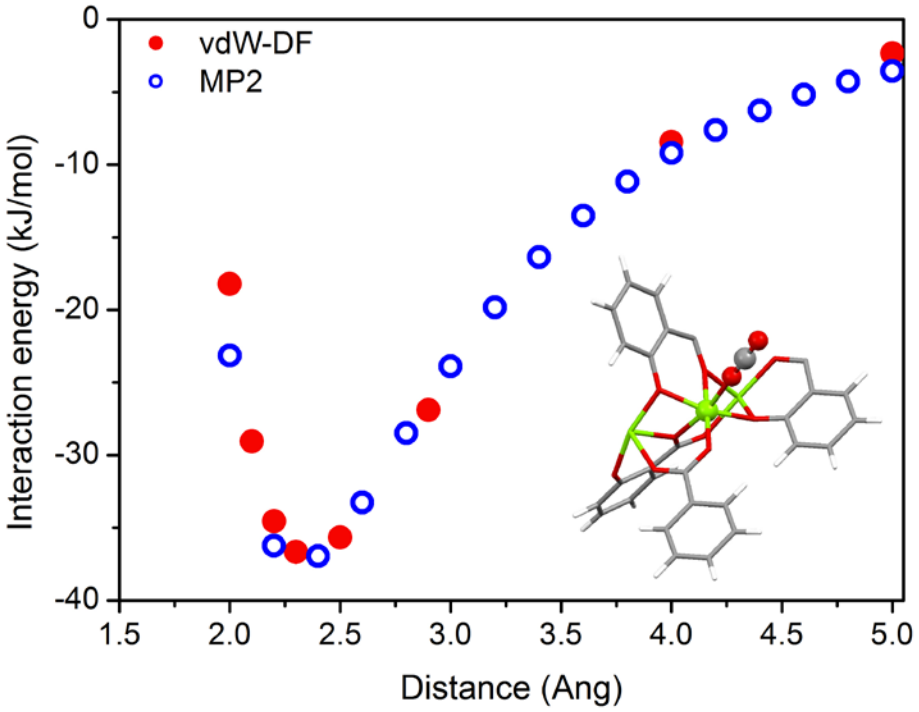

Figure SI 2: Comparison of the interaction energies from the vdW-DF and MP2 calculations between a CO_2 molecule and the shown cluster.

1.5 NEMO decomposition

The partitioned contributions to the interaction energy are computed by a similar (truncated) version of the formula presented by Holt et al.[11] Prior to the calculation of the partitioned contributions, the LoProp properties are simplified. The polarizabilities are made isotropic, the dipoles are modified to reproduce the molecular quadrupole, and the quadrupoles are deleted.

The electrostatic energy contribution E_{elec}, polarization energy contribution E_{pol}, and dispersion energy contribution E_{disp} are given by Equations (2)-(4), where T is the interaction energy tensor (see Stone).[12] Indices A and B are associated with either MOF or guest molecules (i.e. no intramolecular contribution), and i,j are atomic sites.

$$E_{elec} = \sum_{i}^{A}\sum_{j}^{B}\left(T^{ij}\left(q^{i}q^{j}\right)+T^{ij}_{\alpha}\left(q^{i}\mu^{j}_{\alpha}-\mu^{i}_{\alpha}q^{j}\right)-T^{ij}_{\alpha\beta}\left(\mu^{i}_{\alpha}\mu^{j}_{\beta}\right)\right) \quad (2)$$

$$E_{pol} = -\frac{1}{2}\sum_{i}^{A}\mu^{i,ind}_{\alpha}F(A)_{\alpha} \quad (3)$$

$$E_{disp} = -\sum_{i}^{A}\sum_{j}^{B}\left(D^{ij}\right)\frac{E_{AB}}{4}\alpha^{i}_{\alpha\beta}\alpha^{j}_{\gamma\delta}T^{ij}_{\alpha\gamma}T^{ij}_{\beta\delta} \quad (4)$$

For E_{elec}, μ are the modified dipoles. To estimate E_{pol}, we use an induced point-dipole model, which is iterated until convergence ($\delta E < 1.0E^{-10}$ a.u.). Equation (3) gives the polarization contribution for molecule A in the presence of B (the same is true for B in the presence of A). Here $\mu_{\alpha}^{i,ind} = \alpha_{\alpha\beta}^{i} F(A)_{\beta}^{total}$ where $\alpha_{\alpha\beta}^{i}$ are the (isotropic) polarizabilities, and $F(A)_{\beta}^{total}$ includes the induction due to permanent moments as well as induced moments. For E_{disp}, it is the same definition for $\alpha_{\alpha\beta}^{i}$ as Equation (3), and E_{AB} is the average molecular excitation energy given by $E_{AB} = \dfrac{E_A E_B}{E_A + E_B}$, where E_A is the ionization energy of molecule A, and D^{ij} is varied such that E_{rep} (Equation (5)) is always positive. The remainder E_{rep} (which behaves exponentially) is given by

$$E_{rep} = E_{\text{int}} - E_{elec} - E_{pol} - E_{disp} \tag{5}$$

where E_{int} is the total from Equation (1). These terms are then grouped for the fitting, such that the total E_{rep} remains constant and is fitted to the Buckingham repulsion (as described in section 3). The leading electrostatic term $T^{ij}\left(q^i q^j\right)$ is kept, where the q charges are those for the periodic framework described in section 1.3. The difference $E_{\text{int}} - E_{rep} - T^{ij}\left(q^i q^j\right)$ gives the total attraction, which accounts for the higher order electrostatic moments, polarization, dispersion, and changes due to replacement of the charges in going to the periodic system. This remainder is fitted to the C and D attractive parameters (as described in section 3).

2 DFT Calculations

2.1 Details of the DFT calculations

Density functional theory (DFT) calculations were used to optimize the crystal structure and to compute the CO_2-MOF interaction energy along some representative paths. Our DFT calculations were performed using the SIESTA,[13] VASP,[14,15] and QuantumEspresso[16] (QE) implementation.

We have tested the validity of the localized-basis set approach (SIESTA) by comparing structural data and energetics with those obtained from a plane-waves approach (QuantumEspresso and VASP). We used the PBE gradient-corrected exchange-correlation functional in SIESTA and VASP while PW91 was employed in QuantumEspresso. Since these two functionals do not account for dispersive forces, we also employed a recent van der Waals functional (vdW-DF)[17] as implemented in SIESTA,[18]in order to properly describe interaction energies.

The QuantumEspresso calculations use Kohn-Sham orbitals and the charge distribution of the outer shell electrons are expanded in the Fourier series up to the plane-waves of the kinetic energy of 35 Rydberg and 420 Rydberg, respectively. The field exerted on the outer electronic shells C [2s2p], O [2s2p], Mg [2p3s3p3d], Zn [4s4p3d], and H [1s] by the inner cores was described by the non-relativistic Vanderbilt ultrasoft core pseudo potentials; non-linear core correction is included in the Zn and Mg pseudo potentials. The integration over the irreducible Brillouin zone was carried out over 2x2x8, and the results were checked for convergence over 4x4x16 Monkhorst-Pack grids. Atomic positions were considered converged when the total force applied to the atoms in the unit cell is less than 0.004 Rydberg/bohr/cell.

VASP calculations use projector-augmented-wave (PAW) potentials to describe the interaction between core and valence electrons. C [2s2p], O [2s2p], Mg [3s3p] and Zn [4p3d] valence electrons are explicitly included in the valence. A plane-waves kinetic energy cutoff of 500 eV is used and the integration over the irreducible Brillouin zone is carried out over a 2x2x8 Monkhorst-Pack grid. Atomic positions are relaxed until forces are lower than 0.02 eV/Å.

SIESTA calculations used variationally optimized double-Z polarized basis sets[19] implying the presence of d-orbitals for C, N and O. Non-local, norm-conserving fully separable Trouiller-Martins pseudopotentials were used. C [2s2p], O [2s2p] and Mg [2s2p3s] electrons were explicitly included in the valence. Real space integrals were performed on a mesh with a 300 Ry cutoff. Geometries were optimized until Hellmann-Feynman forces were smaller than 20 meV/Å. For the interaction energy with CO_2, a counterpoise correction was applied to correct for basis set superposition error. A 2x2x8 Monkhorst-Pack grid was used for the integration over the irreducible Brillouin zone. The integration over the irreducible Brillouin zone is carried over 64 grid points.[20]

2.2 Crystal structure calculations

In our calculations we relied on an accurate representation of the crystal structure of Mg-MOF-74. Unfortunately at present, single crystals of Mg-MOF-74 have not been obtained and the structural information is therefore obtained from powder diffraction data[21-23] Detailed inspection of these experimental structures shows a significant distortion of the bridging ligand in powder diffraction data (Mg-MOF-74), which is not observed in our DFT calculations.

We used PW91 (QE) and PBE (SIESTA and VASP) to obtain the fully relaxed structure of the MOF. The good agreement between these two approaches confirms the validity of the localized basis set approach employed within SIESTA. The lattice parameters and the C-C bond lengths within the ligand of the relaxed geometry obtained with PW91 (QE) and PBE (SIESTA and VASP) are reported in Table SI 1. Similar results were obtained with D3LYP by Valenzano et al.[24] The fact that four different approaches predict nearly identical crystal structure gives us confidence in the reliability of the theory. It is therefore surprising that a comparison with the experimental structure show such large deviations. For example, we found a deviation of the C_a-C_b and C_d-C_b bond distances by as much as 8% and 7%, respectively.

As we are interested in predicting the adsorption isotherms, we computed the adsorption isotherms of CO_2 for the experimental structure and the structures predicted by DFT (see Figure SI 3). The results show that the two different DFT structures (PW91) and (PBE) give nearly identical adsorption isotherms. But the results differ from the experimental isotherm. These differences illustrate the importance of using the correct Mg-MOF-74 structure.

For Zn-MOF-74, a closely related material, it is possible to synthesize a single crystal and for this material crystal structure can be determined with higher accuracy.[22] In Table SI 1 we have compared the structural data for this material from our DFT (PW91, QE and PBE, VASP) calculations, previous calculations,[24] and experiments.[21,23] For this material our calculated lattice parameters and atomic positions are in an excellent agreement with the experimental data (the largest deviation for C_a-C_b bond length is 1.2%).

Given the uncertainties with the experimental structure for Mg-MOF-74 and the excellent agreement we obtained using our DFT approach for Zn-MOF-74, we conclude that the computational structure of DFT is most likely the most reliable representation of Mg-MOF-74. The PBE-VASP structure is therefore used in this work for all our calculations of adsorption isotherm.

For the extended MOF-74 structure, the PBE-VASP lattice parameters for Mg and Zn are a=21.897 Å and c=6.938 Å, and a=21.933 Å and c=9.924 Å, respectively. A good agreement is found with available single crystal data for Zn (a= 21.698 Å and c=6.869 Å).[25]

Table SI 1: Comparison of structural parameters between this work and previous experimental and computational studies. C_a-C_b, C_b-C_c, C_c-C_d and C_d-C_b correspond to bond lengths between C atoms within the ligand reported in Figure SI 1. Distances are in Angstrom (Å).

Metal, method	Lattice parameters		Bond lengths			
	A	c	C_a-C_b	C_b-C_c	C_c-C_d	C_d-C_b
Mg, this work (PW91, QE)	26.114	6.917	1.483	1.433	1.399	1.401
Mg, this work (PBE, SIESTA)	26.260	7.036	1.490	1.436	1.405	1.406
Mg, this work (PBE, VASP)	26.136	6.942	1.484	1.434	1.401	1.402
Mg, DFT-B3LYP, (Valenzano[24])	26.109	6.969	1.493	1.430	1.396	1.399
Mg, exp., (Dietzel[23])	26.026	6.759	1.540	1.314	1.430	1.509
Mg, exp., (Queen[21])	25.922	6.863	1.613	1.490	1.526	1.260
Zn, this work (PW91, QE)	26.095	6.888	1.482	1.430	1.397	1.400
Zn, this work (PBE, VASP)	26.190	6.935	1.484	1.432	1.399	1.402
Zn, exp., (Rosi[22])	25.932	6.837	1.500	1.420	1.391	1.398

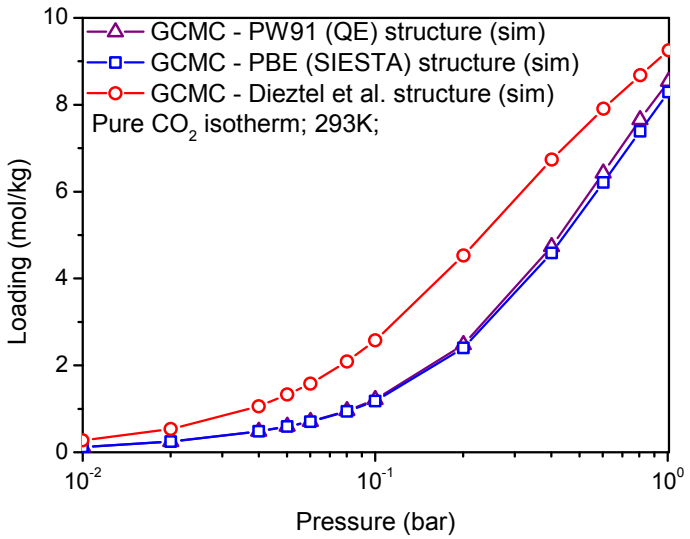

Figure SI 3: Effects of the crystal structure on the adsorption isotherms for CO_2 at 293K. We compared the experimental structure of Dietzel et al[23] with the DFT optimized structures (both QE and Siesta) The grand canonical Monte Carlo simulations use the Universal force field[9] and the TraPPE force field[26] with the Lorentz-Berthelot mixing rules to describe the CO_2 - MOF and CO_2 – CO_2 interactions.

2.3 CO_2 – MOF interactions

The interactions between CO_2 and the MOF are calculated using the SIESTA package. The binding energy of n CO_2 molecules with the framework is computed as:

$$E_B = E\ (MOF + n\ CO_2) + E\ (MOF) - n\ E\ (CO_2)$$

and basis set superposition error was counterpoise corrected. The computed CO_2-MOF binding energy for a fully loaded ($1CO_2$: 1Mg) MOF was 21.32 kJ/mol and 42.55 kJ/mol with PBE and vdW-DF, respectively. The difference between these two numbers is related to the van der Waals interactions, which are not included in PBE. Results similar to our PBE binding energies were obtained with our PW91 (QE) plane waves calculations, i.e. 24.12 kJ/mol. This is consistent with the similar parameterization for the exchange and correlation of these two functionals. These numbers compare well with the B3LYP (19.2 kJ/mol) and B3LYP+D (42.5 kJ/mol) calculations of Valenzano et al.[24], where the B3LYP+D method uses the approach of Grimme[27] for the van der Waals interactions. Also, Wu *et al*.[28] computed LDA and PBE binding energies of 51.2 kJ/mol and 20.2 kJ/mol.

Binding energies and geometries are reported in Table SI 2 and show a good agreement between this work and previous computational studies.[28] Also, the computed CO_2 arrangement within the unit cell was confirmed by structural data for Mg-MOF-74.[21,28]. Also, we computed the CO_2-MOF binding energy at a smaller loading, i.e. $1CO_2$: 6Mg, and a value of 41.30 kJ/mol is found with vdW-DF, showing a favorable contribution from CO_2-CO_2 intermolecular interactions of 1.25 kJ/mol.

A lower CO_2-MOF binding energy is found for Zn-MOF-74 compared to Mg-MOF-74, in agreement with previous calculations[20]. Results are shown in Table SI 2. For instance, a vdW-DF binding energy of 34.13 kJ/mol is found here for a fully loaded MOF in good agreement with the value of 35.2 kJ/mol reported by Valenzano[20].

The computed interaction energies (vdW-DF) along two different paths within the Mg-MOF-74 are presented in Figure 2 of the article. These data are used to validate the accuracy of our proposed force field in a periodic system.

Table SI 2: Computed CO_2 binding energies and geometries (The distance between the metal and the closest oxygen of CO_2 (Mg-O (CO_2)), the bond angle between the metal and CO_2 (M-O-C), and the CO_2 bond angle (O-C-O)).

	E_B (kJ/mol)	M-O (CO_2) (Å)	M-O-C (deg)	O-C-O (deg)
$1CO_2$: 1Mg, this work (PW91, QE)	24.12	2.371	132.6	178.2
$1CO_2$: 1Mg, this work (PBE, SIESTA)	21.32	2.332	130.7	177.1
$1CO_2$: 1Mg, this work (vdW-DF, SIESTA)	42.55	2.354	128.2	177.6
$1CO_2$: 1Mg, (Valenzano[24]), B3LYP	18.20	2.351	131.4	178.2
$1CO_2$: 1Mg, (Valenzano[24]) B3LYP+D	41.50	2.310	129.4	178.0
$1CO_2$: 1Mg, (Wu[28]) PBE	20.20	2.396	136.6	178.7
$1CO_2$: 1Mg, (Wu[28]) LDA	51.20	2.208	136.5	175.0
$1CO_2$: 6Mg, this work (vdW-DF, SIESTA)	41.30	2.326	132.0	177.4
$1CO_2$:1Zn, this work (vdW-DF, SIESTA)	34.13	2.564	122.5	178.2
$1CO_2$:6Zn, this work (vdW-DF, SIESTA)	32.00	2.577	122.2	178.7
$1CO_2$:1Zn, B3LYP+D (Valenzano[20])	35.20	2.491	121.2	178.3

3 Force field parameterization

Mg-MOF-74 is composed of four different elements: Mg, O, C, and H. Due to its bonding environment, different atoms of the same element require separate parameterization in the force field to accurately reflect its local environment. We denote these distinct atom environments using the names Mg, O_a, O_b, O_c, C_a, C_b, C_c, and C_d (see Figure SI 1 in section 1.2). We did not consider the H explicitly.

We used the procedure below to obtain pair-wise interaction parameters for each of these atoms with N_2 and CO_2. Tests have shown that the influence of the parameters for the carbon atom of CO_2 on the predicted adsorption behavior was very small, and variations by as much as 30% of the Universal force field parameters[9] had a negligible effect on the adsorption isotherms. Therefore, we only refined interactions between the oxygens of CO_2 and the atoms of the MOF.

For each type of atom, an appropriate cluster was determined (see section 1.2). In order to fit the parameters for a particular pair-wise interaction separately, it is important to determine a set of configurations that is dominated by the interaction with the specific atom type of interest. Paths composed of several configurations were generated using the Universal force field for the framework atoms and TraPPE force field[26] for guest molecules (CO_2 or N_2). The orientation of this approaching molecule was calculated by minimizing the repulsive energy between the guest molecule and atoms of the cluster, excluding the atoms with the specified atom type for that cluster. This procedure ensured that the repulsive interaction between the guest molecule and the atoms of the specified atom type dominates the total repulsive energy. Based on the 12-6 Lennard-Jones potential, paths with the minimized repulsive energies (12^{th} order term) between the guest molecule and atoms of the cluster, excluding the atoms with the specified atom type for that cluster, will also have the minimized attractive energies (6^{th} order term), and the same paths can be used to explore both parts of the potential.

For an each configuration on a given path of a guest molecule around a cluster, a MP2 calculation and NEMO decomposition were performed to get the individual components of total interaction energy (see section 1). The repulsion energy and attraction energy were identified for each path with a given guest molecule and were used to build the new force field using the fitting procedure proposed below. In the new force field, a modified Buckingham potential model, Equations (6) and (7) was used to describe the repulsion and attraction energy between the structure and the end atoms of the guest molecules, respectively.

$$u^{rep}(r) = \begin{cases} \infty & r < r_{\min} \\ A\exp(-Br) & r > r_{\min} \end{cases} \tag{6}$$

$$u^{att}(r) = \frac{C}{r^5} + \frac{D}{r^6} \tag{7}$$

As mentioned above, the repulsion energy between the guest molecule and the target atom type in its corresponding cluster was designed to be the dominant component of the total repulsion energy. The interaction energy between the target atom and the end atoms of the guest molecule can be regarded as the most important component of the total energy. Consequently, during the parameterization procedure only the force field parameters for the interaction between the target atom type and the guest molecule were adjusted to minimize the norm of the difference between NEMO-decomposed repulsion energy and calculated repulsion energy.

Initial guesses for all pair-wise interactions were taken from the Universal force field[21] and TraPPE force fields[26] with the Lorentz-Berthelot mixing rules. The fitting was carried out in two phases. To improve the initial guess, we first took all atoms of a particular element (all O atoms or all C atoms) and simultaneously minimized the error over all paths for that element. This adjustment was done in the order: Mg, O, and C. These parameters were used as the initial guesses for the second phase, where we optimized the force field parameters for each atom type individually with an ordering based on its relative contribution to the total repulsion energy. The ratio of the repulsion energy of the target atom type and the guest molecule to the total repulsion energy was computed, and the paths were taken in order from the highest to lowest ratio. This procedure was repeated iteratively until all the parameters were converged. For the fitting to attractive part of the potential, the procedure is exactly the same as the one described above for the repulsive part, using the same paths identified above. For these parameters, however, we set the attractive interaction between the interior atom of the guest molecule and the framework atoms to be zero.

Figure SI 4 demonstrates that our new force field reproduces the NEMO-decomposed MP2 energies very well for the Mg-MOF-74 structure.

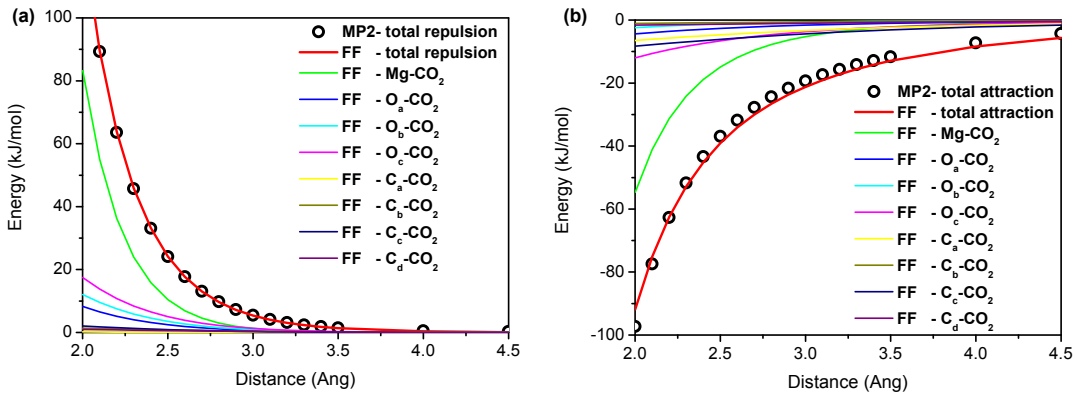

Figure SI 4: Typical result for the NEMO fitting. The left figure (A) shows the fit for the repulsive interactions between CO_2 and the cluster for the Mg path for Mg-MOF-74. The right figure (B) shows the attractive part of the energy. The legends show the contribution of the various energies to the total energy, and illustrate that the path are dominated by the CO_2-Mg interactions.

4 Molecular simulations

To compute the thermodynamic properties we used grand canonical Monte Carlo (GCMC) and canonical Monte Carlo simulation to compute adsorption isotherms and to characterize the adsorption properties.

4.1 Force fields

In our simulations we used a hybrid force field. The interactions of the guest molecules were described with the TraPPE force field[26] for guest molecules (CO_2 and N_2). The interactions between the guest molecule and framework atoms were described with the modified Buckingham potential model. The detail methodology to obtain the force field is introduced in the section 3, and the parameters are summarized in the section 9.

4.2 Simulation details

In the GCMC simulation, configurations of molecules inside the pore space of the material are generated by random (re-) insertion, deletion, and translation of individual molecules within a simulation box composed of multiple unit cells of the material. Electrostatic energy was computed using the Ewald summation technique. Short-range interactions were cut off and shifted to zero at a distance of 12.8 Å. The simulation box extended at least twice this distance in all orthogonal directions. To accelerate the calculation of molecule-framework interaction energies, the short-range part of the interaction was stored in a pre-computed grid with a spacing of 0.10 Å and linearly interpolated between grid points. The number of equilibration steps is set to 20 million MC cycles while the production cycles is set at 2.4 million.

To save CPU-time all of the interactions between the gas-host atoms are stored inside the energy grid, which were computed before the start of the GCMC simulations. Additionally, the reciprocal space contributions of the Ewald summations that describe the interactions between guest molecules and guest molecules are stored inside a second energy grid to expedite the calculations further.

To further expedite these simulations, we utilized graphics processing units (GPUs) to conduct the GCMC simulations. All of the simulations were conducted on the Dirac cluster at NERSC, which consists of Fermi Tesla C2050 cards. In a single simulation, fourteen independent GCMC simulations at different pressure values are processed, with the number fourteen chosen to correspond to the total number of streaming multiprocessors available in the C2050 cards.

5 Study of extended Mg-MOF-74 (Mg_2(dobpdc))

The purpose of this section is to demonstrate the transferability of the force field. In this section we show that the parameters we have obtained for the dobdc linker in MOF-74 can be used in a related material with a slightly different (dobpdc) linker.

5.1 Description of the system

Mg_2(dobpdc) has a structure similar to Mg-MOF-74. The main difference is that the linker in MOF-74 (dobdc) is replaced by an extended linker (dobpdc). The structure is shown in Figure SI 5 together with our convention for naming the atom types. For the extended linker here, all oxygen types are assigned identically, while we now have more C_b and C_d types per linker. These are not all chemically equivalent by symmetry. However, our calculations show that the differences are small and hence these atoms can be described using the same force field.

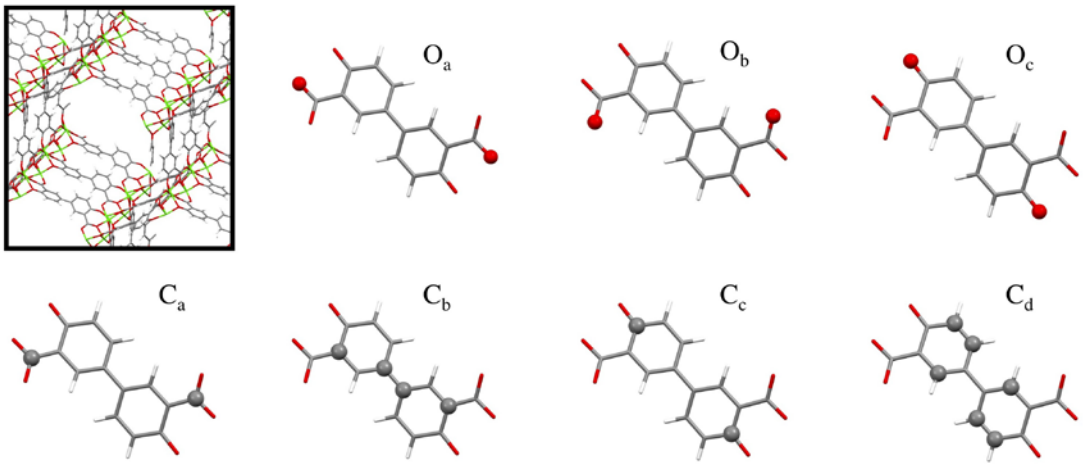

Figure SI 5: Image of Mg_2(dobpdc) (left) where it is shown that all Mg types are equivalent. The three oxygen atom-types and four carbon atom-types are shown, along with the same naming scheme as for MOF-74.

5.2 CO_2 adsorption isotherms

To obtain the force field we recalculated the charge distribution for the Mg_2(dobpdc) structure. The other parameters we taken directly form the force field developed for Mg-MOF-74 (see section 9 for all the parameters).

In Figure SI 6 we compare our predicted isotherms with the experimental data reported by McDonald *et al.*[25] The predicted isotherm agrees very well with the experimental one. It is important to mention that while for Mg-MOF-74 only 80% of the Mg sites were available, in the extended Mg-MOF-74 structure, almost all the Mg sites are available. This explains why we have for this material a much better agreement at higher loading.

In addition, we have tested the sensibility of the charges on the framework atoms. Figure SI 7 shows that the computed isotherms with new calculated charges (see section 1) and the charges adopted from Mg-MOF-74 directly are almost identical. It is important to note that the charges on the hydrogen atoms were slightly adjusted to ensure that the entire framework is neutral. The new computed charges for this system are summarized in the section 9.

It is interesting to see whether similar to MOF-74, this material also has an enhancement of the adsorption because of the CO_2-CO_2 interactions. Figure SI 8 clearly illustrates that the collective effect in this extended system is far less pronounced. Because the linkers are longer, the CO_2-CO_2 interactions are less important in this material and we observe a normal Langmuir behavior.

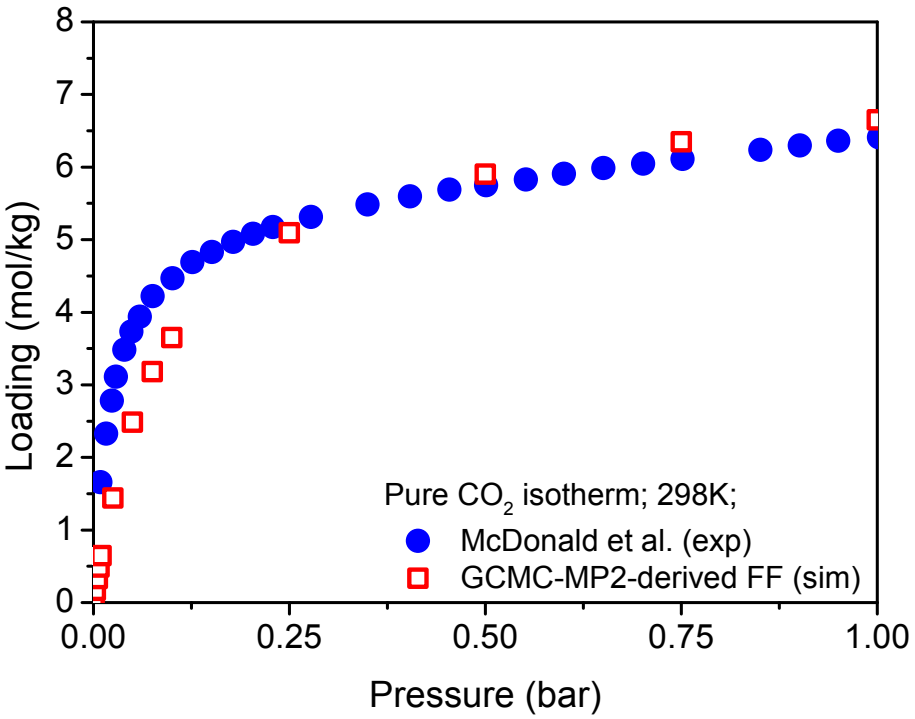

Figure SI 6: Simulated and experimental isotherm at room temperature (298K). Closed symbols shows the experimental CO_2 isotherms in extended Mg-MOF-74 at 298 K. The open red symbol shows the adsorption isotherm calculated with MP2-derived force field.

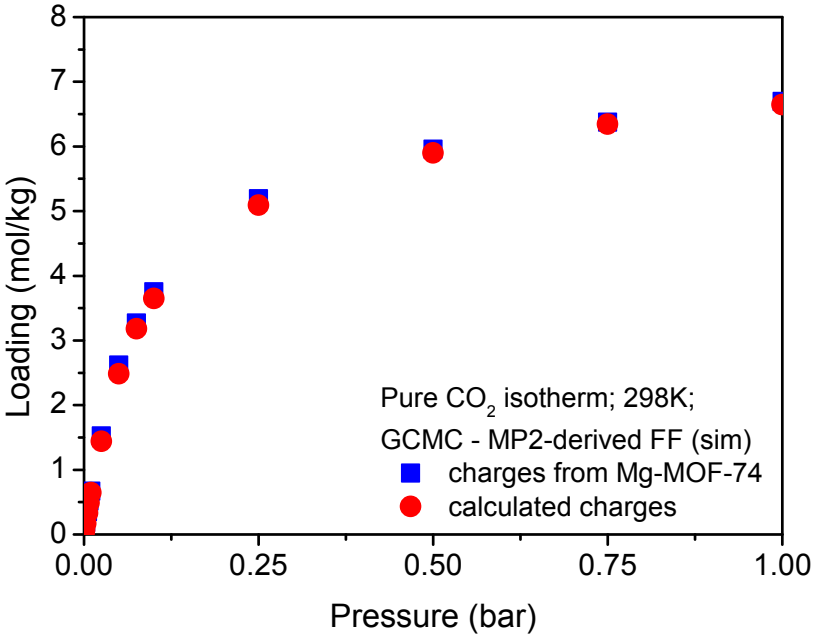

Figure SI 7: Simulated CO_2 isotherm in Extended Mg-MOF-74 with different charges. The blue closed squares show the calculated isotherm with the charges taken directly from Mg-MOF-74. The red circles show the simulation result with the recalculated charges for this system.

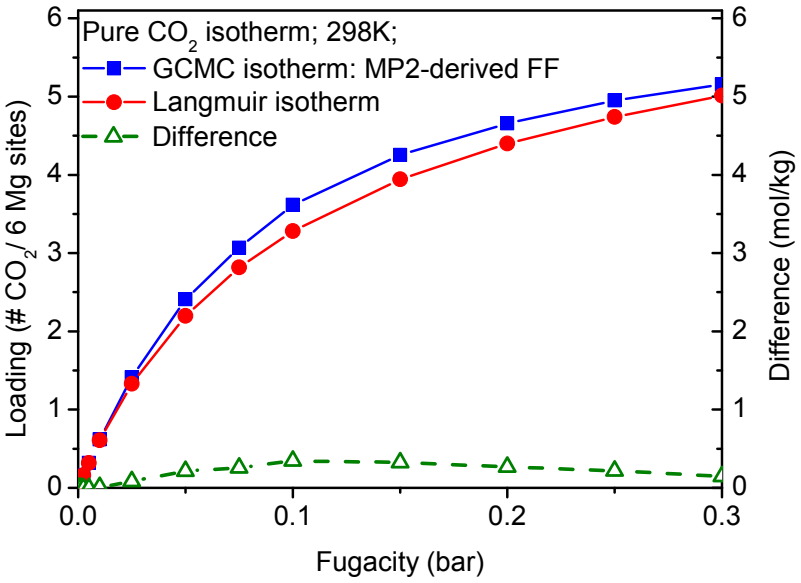

Figure SI 8: Enhancement of the adsorptions of CO_2 as a function of loading in extended Mg-MOF-74. The comparison between a Langmuir isotherm (red) with the results from GCMC simulations (blue). The parameters of the Langmuir isotherm are obtained from the Henry coefficient from the GCMC simulations and the maximum loading, which is set to one CO_2 per Mg site. The difference between these curves (green) indicates the enhancement induced by the presence of other CO_2 molecules.

6 Replacement of Mg with a different Metal (Zn-MOF-74)

Here we test the transferability of the force field between two nearly identical structures with a different metal site (Zn-MOF-74 versus Mg-MOF-74). In this section, we used the same procedures for Zn-MOF-74 as for Mg-MOF-74, including the structure relaxation by DFT, the assignment of atom-types, the determination of the approaching guest paths followed by MP2 interaction energy calculation, and the subsequent Nemo decomposition.

6.1 Force field development

Both Mg-MOF-74 and Zn-MOF-74 are composed of the same dobdc organic linker; the only difference between these structures is the metal site. Figure SI 9 (A) and (B) show the comparison of the MP2 decomposed van der Waals energies for all paths between Mg-MOF-74 and Zn-MOF-74. Given that the clusters of all atom types and their corresponding approaching paths in both structure are almost identical, this comparison illustrates that only the metal path is dramatically affected by the replacement of the Mg by Zn, while all other atom-types are much less affected. This indicates that a very reasonable isotherm can be obtained if we only replace the metal-guest interactions. For the Zn-MOF-74 oxygen and carbon force field, we can use the corresponding values of Mg-MOF-74. Figure SI 9 (C) and (D) show that the force field for Zn-MOF-74 can reproduce the MP2 energies for all paths, and give almost identical fitting accuracy to the Mg-MOF-74 case (Figure 1 (C) and (D)). All the force field parameters used in Zn-MOF-74 are summarized in the below section 9.

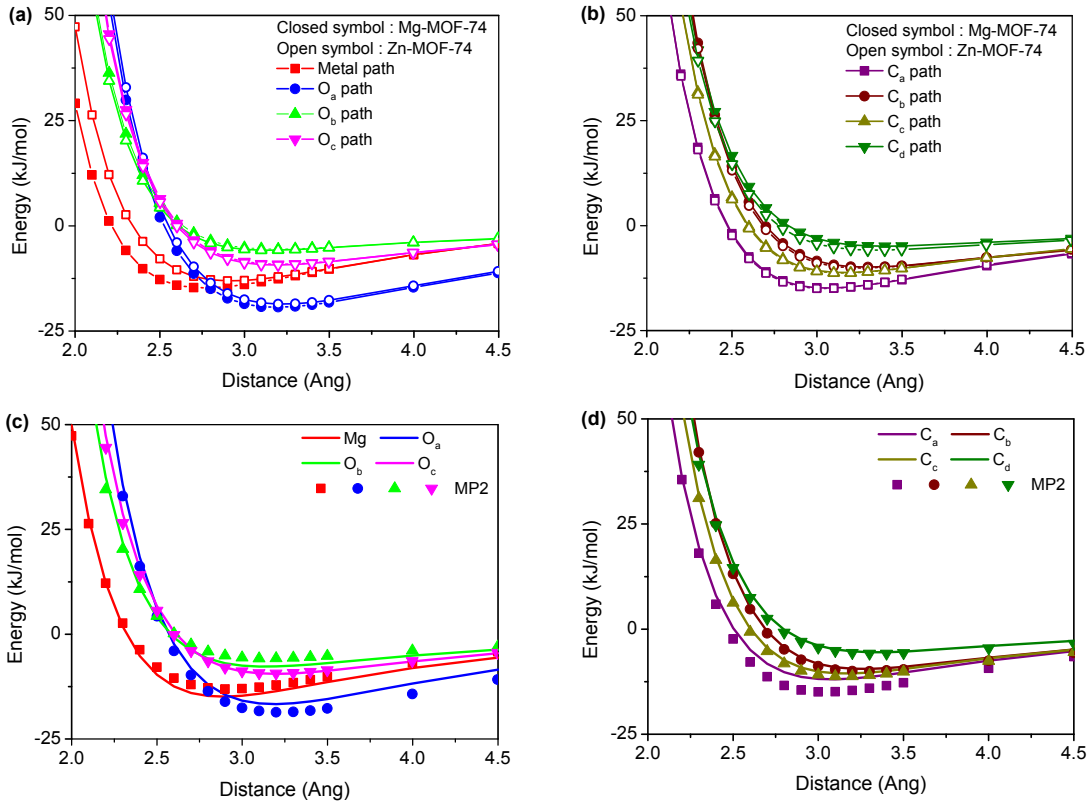

Figure SI 9: (A) and (B): Comparison of MP2 decomposed non-bonded energies (excluding the electrostatic contribution) between Mg and Zn cases for all the paths. The closed symbols are the Mg-MOF-74 results and the open symbols are the Zn-MOF-74 results. (C) and (D): Comparison of the MP2 repulsive plus attractive energies for the eight different paths (given by closed symbols) with the results from the force field (solid lines).

6.2 Prediction of the CO_2 adsorption properties

The predicted pure component CO_2 isotherms were obtained with the MP2-derived force field at 313K and shown in Figure SI 10. Experimental isotherm in the lower pressure region was reported by Caskey et al,[29] however, their measurement also showed N_2 saturation loading significantly lower for Zn-MOF-74 compared with Mg- and Ni-MOF-74 cases. This indicates that the sample (Zn case) was much more difficult to activate compared to the other structures, which makes it difficult to make a direct comparison with experimental data for this material.

Given these experimental uncertainties it is important to compare the simulated Mg-MOF-74 and Zn-MOF-74 isotherms (see Figure SI 10). We observe a steeper uptake as a function of pressure in the Mg case compared to Zn. This result implies that the binding energy of CO_2 in Mg-MOF-74 should be larger in magnitude than CO_2 in Zn-MOF-74, which we also show to be the case by calculating the heat of adsorption at the infinitely diluted condition. Our calculated heat of adsorption of 31.8 kJ/mol at 298K is comparable to the value reported by DFT of CO_2 in Zn-MOF-74,[24] which is close to the experimental value of ~30 kJ/mol reported by Simmons et al.[30] It is worth noting that our

simulation results of CO_2 heat of adsorption Zn < Mg is consistent with those obtained from DFT calculations.[24]

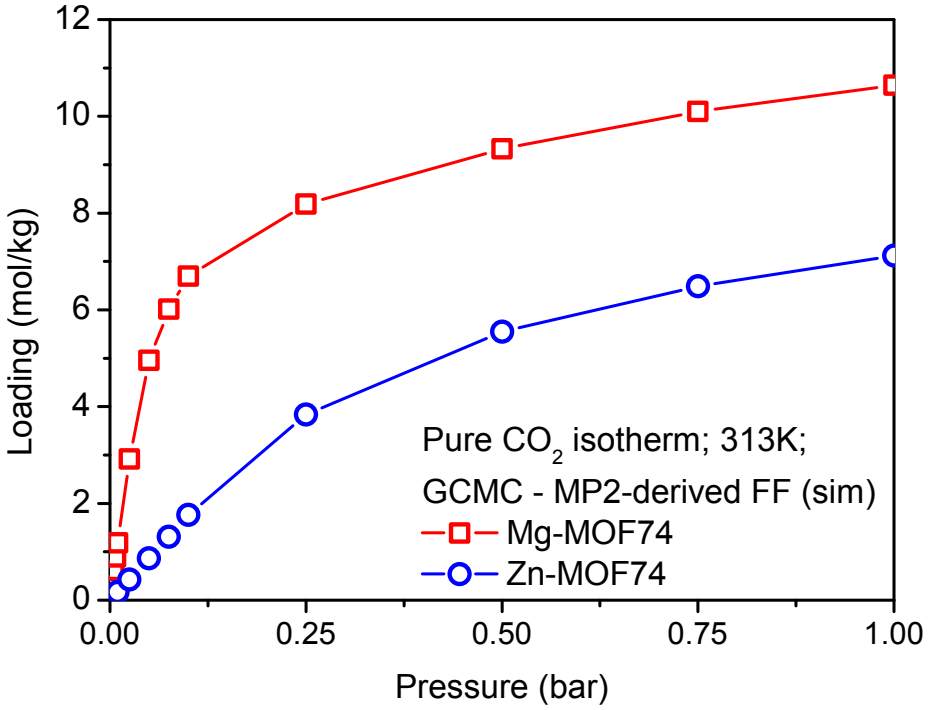

Figure SI 10: Simulated isotherm at 313K for both Mg-MOF-74 and Zn-MOF-74. The red open square symbols show the simulated CO_2 isotherms in Mg-MOF-74 and the blue open circle symbols give the isotherm of CO_2 in Zn-MOF-74.

7 Extend to general structure (MOF-5)

Until now we have focused on materials with open metal sites. For these materials the conventional force fields fail to describe the adsorption isotherms. As in these materials the open metal site are dominating the adsorption process, it is important to test that our methodology also is applicable for materials that do not have such an open metal site. Therefore we have applied out methodology also to MOF-5, which is well-studied (non open-metal site) material.

7.1 Description of the system

Atom types for the framework of MOF-5 were defined based on the symmetry of the periodic system, which has 7 distinct atom types. All M_4O connectors are equivalent (Zn, O_{cent}), and each benzenedicarboxylate (bdc) linker has one type of oxygen atom (O_{ab}), 3 types of carbon atoms (C_a, C_b, and C_d), and 1 type of hydrogen (H) shown in Figure SI 11. The naming scheme adopted for the organic linker is analogous to the MOF-74 case, except as is shown in Figure SI 1 there is no analogous O_c or C_c atom-type, and previous O_a and O_b are now chemically equivalent.

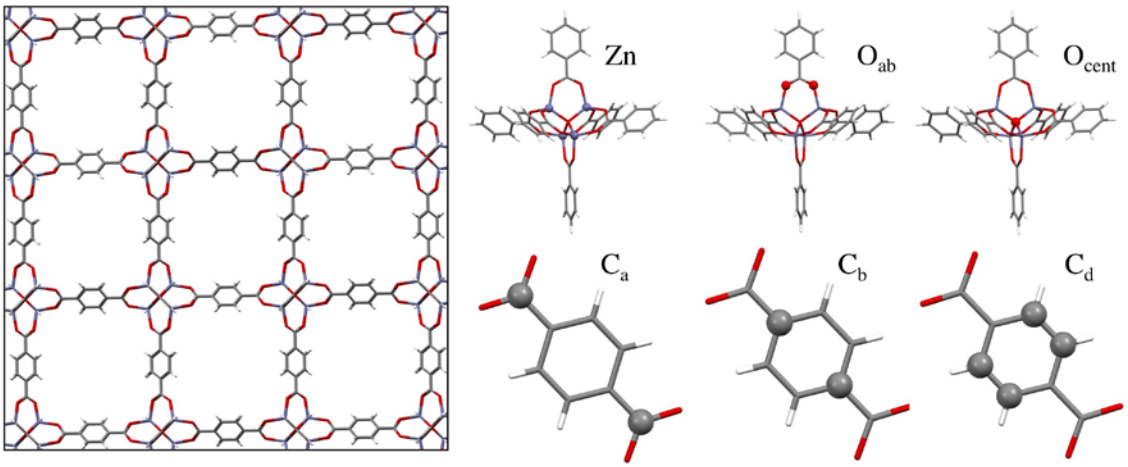

Figure SI 11: Image of MOF-5 structure (left) and the 6 unique atom-types (excluding H) along with the naming scheme adopted here.

The charges and interaction energies were obtained using the methodology described in section 1. The clusters with CO_2 approaching are shown in Figure SI 24-26 in section 10. For this system, we took Zn and O_{cent} parameters for dispersion directly from the UFF force field since these two atom types are embedded inside the surface of the framework. Because of this, the CO_2 cannot directly approach these two atom-types, but also the dispersive interaction between CO_2 and these atom-types is far less important.

7.2 Prediction of the CO_2 adsorption isotherm

The MP2-derived force field was tested by comparing the predicted pure CO_2 adsorption isotherms with the experimental isotherms at various temperatures published in the

literature[31] . For the room temperature (298K) that is relevant for carbon capture, Figure SI 12 clearly shows the calculated isotherm with MP2-derived force field is in a very good agreement with the experimental result. In addition, pure CO_2 adsorption isotherms at 5 different lower temperatures were also computed and then compared to the experimental result. Figure SI 13 illustrates that this new MP2-derivded force field can be used to predict the isotherms at low temperatures in MOF-5. Although the transition point shown in the isotherms at 208K and 218K were not captured perfectly by our force field, the uptake before the phase transition is reproduced very well. From this, we can confirm that our methodology is not only applicable to open-metal site MOFs, but it is also able to obtain a sensible force field for a general material (MOF-5 in this case). All the force field parameters were summarized in the following section 9.

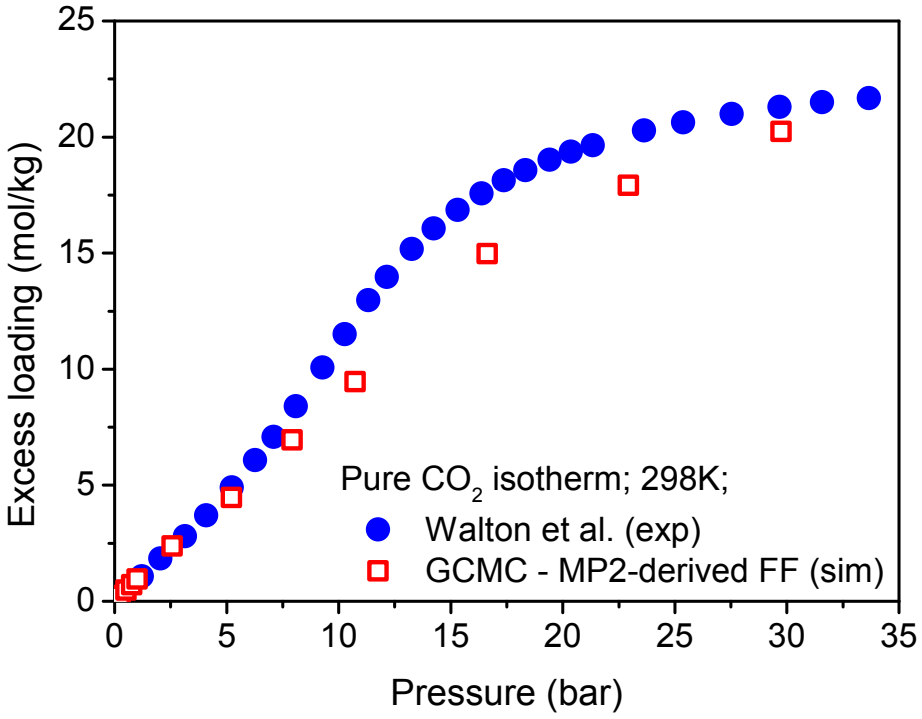

Figure SI 12: Simulated and experimental isotherm at room temperature. Closed symbol shows the experimental CO_2 isotherms in MOF-5 at 298 K. The open red symbol shows the adsorption isotherm calculated with MP2-derived force field.

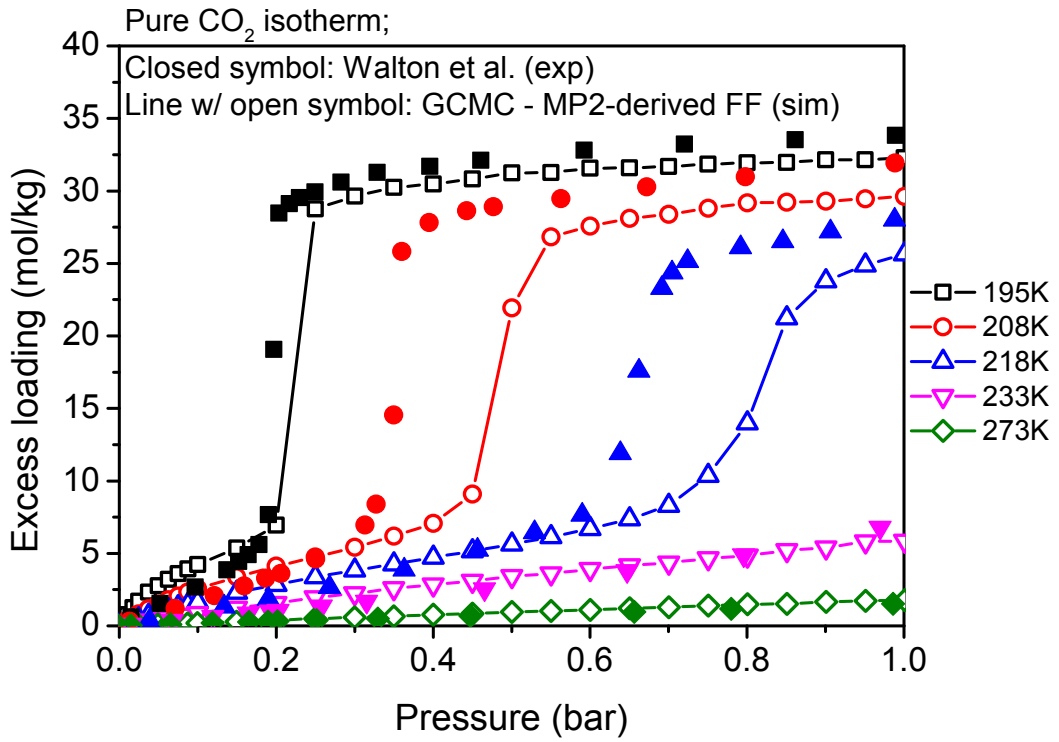

Figure SI 13: Simulated and experimental isotherm at five low temperatures. Closed symbol shows the experimental CO_2 isotherms at several low temperatures. The corresponding color with open symbol (with solid line) shows the adsorption isotherm calculated with MP2-derived force field.

8 Mixture isotherm predictions

Adsorption isotherms of a 14:86 CO_2:N_2 mixture at flue gas conditions (313 K) in Mg-MOF-74 were computed by using the grand canonical Monte Carlo (GCMC) simulation technique with the force field proposed in this work. Figure SI 14 shows the computed mixture isotherms over a wide range of total bulk gas fugacities.

The GCMC-predicted mixture isotherms were used as a benchmark to test the applicability of ideal adsorbed solution theory (IAST).[32] The GCMC technique was also applied to compute the pure component isotherms of CO_2 and N_2 in Mg-MOF-74 at 313K, which are required inputs for IAST. To facilitate the integration of the IAST model, the pure CO_2 isotherm was fit using the dual-site Langmuir isotherm (Equation (8)) while the single-site Langmuir isotherm model (Equation (9)) was used for pure N_2 isotherm. Parameters for the isotherm fits are shown in the figure SI 15 and table SI 3 below. Figure SI 14 demonstrates that the mixture isotherms predicted by IAST are in excellent agreement with the mixture isotherms computed by GCMC simulations over a very wide range of fugacities. At very low fugacities, there is a small discrepancy between the predictions of IAST and the GCMC simulations. This disagreement is due to the observed enhancement in the adsorption of CO_2 we have pointed out in the article. Thus, a small discrepancy is also observed in the fitting to the isotherm of pure component CO_2.

$$q_{CO_2} = \frac{K_1^{CO_2} f_{CO_2}}{1 + \frac{K_1^{CO_2}}{q_{sat,1}^{CO_2}} f_{CO_2}} + \frac{K_2^{CO_2} f_{CO_2}}{1 + \frac{K_2^{CO_2}}{q_{sat,2}^{CO_2}} f_{CO_2}} \quad (8)$$

$$q_{N_2} = \frac{K_1^{N_2} f_{N_2}}{1 + \frac{K_1^{N_2}}{q_{sat,1}^{N_2}} f_{N_2}} \quad (9)$$

In the equations above, K^i is the Henry coefficient, q^i is the loading, and f_i is the partial fugacities of the components.

To the best of our knowledge, mixture adsorption isotherms have not been measured for this system, but they are important for determining the performance of a material for carbon capture. Our calculations have illustrated that IAST predicts the mixture isotherms accurately from the pure component isotherms in Mg-MOF-74. Without GCMC simulations using our accurate force field, it is difficult to validate the predictions of IAST for this material.

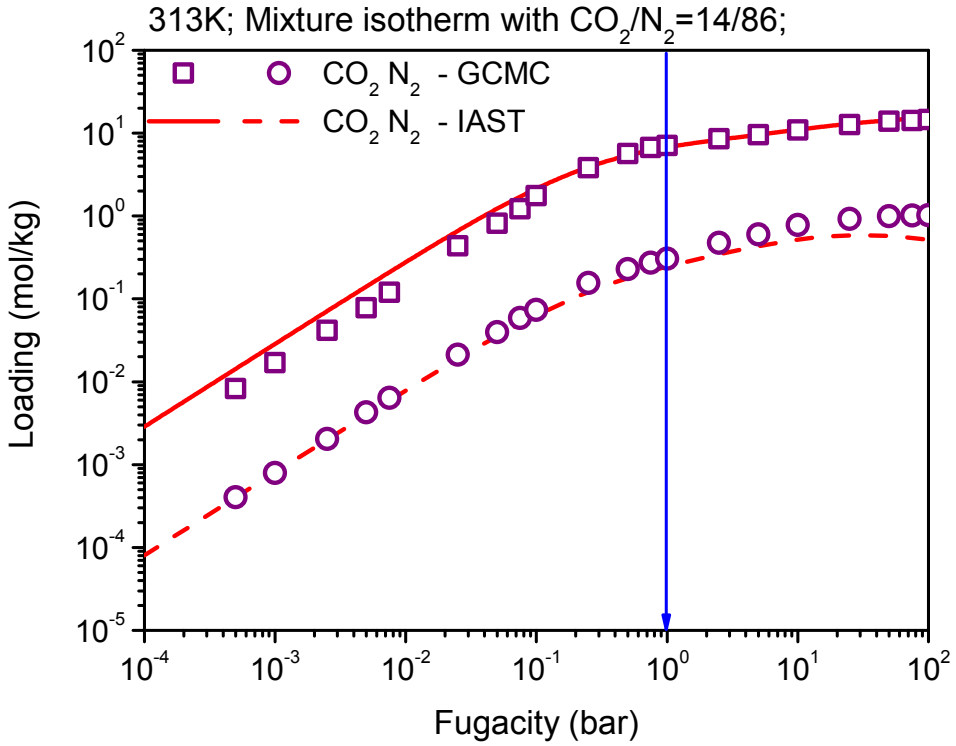

Figure SI 14: Simulated and predicted mixture isotherm. Open symbol shows the CO_2/N_2 (14/86) mixture isotherms in Mg-MOF-74 at 313K. The red line shows the mixture isotherm predicted by IAST. The blue arrow indicates the flue gas condition.

Table SI 3. Parameters of the Langmuir isotherm model for the pure component CO_2 and N_2 isotherms at 313K in Mg-MOF-74. The saturation loading for the first adsorption site of the pure component CO_2 isotherm was directly calculated by assuming all Mg sites are available, that is, one CO_2 per one Mg site.

Component	Langmuir model parameters			
CO_2	K_1 (mol//(kg*Pa))	$q_{sat,1}$ (mol/kg)	K_2 (mol//(kg*Pa))	$q_{sat,2}$ (mol/kg)
	2.01E-03	8.24	3.91E-05	8.93
N_2	K_1 (mol/(kg*Pa))		$q_{sat,1}$ (mol/kg)	
	9.38E-06		12.50	

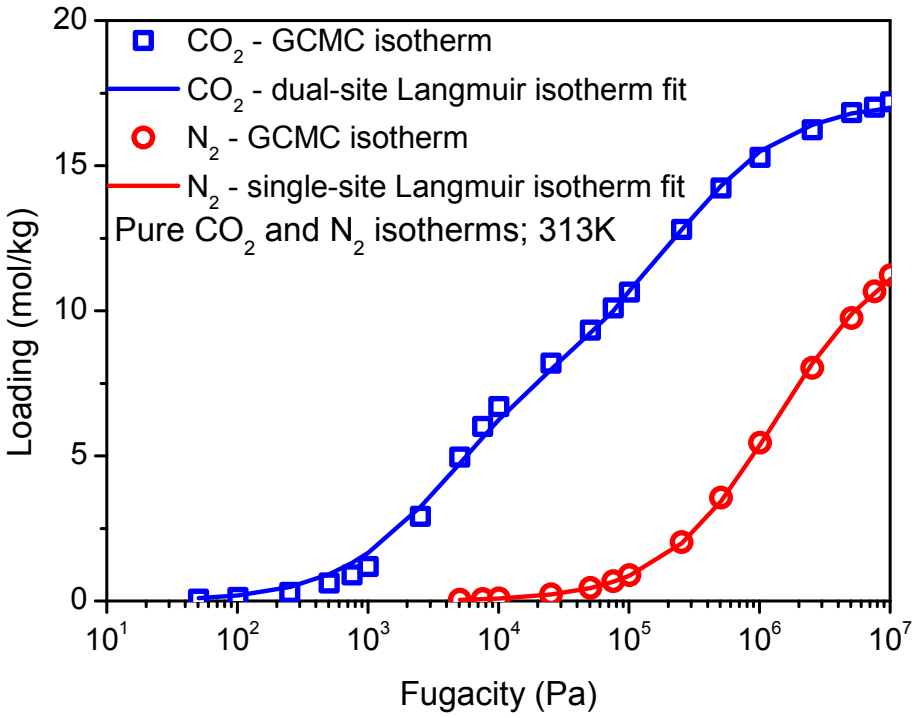

Figure SI 15: Fitting results of the Langmuir isotherm model to the pure component isotherms. Open symbol shows the pure component CO_2 and N_2 isotherms in the Mg-MOF-74 at 313K. The solid lines show the fitting results to the isotherms by assuming the (dual- or single-) Langmuir isotherm model.

9 Summary of force field parameters

Pairwise potential parameters for the modified Buckingham potential model (See section 3), Lennard-Jones potential model, and atomic partial charges are summarized in the tables below. Table SI 4-6 gives the repulsion (A, B) and attraction (C, D) parameters of the interactions between the MOF and CO_2. Table SI 7 gives the repulsion (A, B) and attraction (C, D) parameters of the interactions between the MOF and N_2. Table SI 8-11 gives the charges for framework atoms. Table SI 12 gives the Lennard-Jones parameters for guest molecules. The Lorentz-Berthelot mixing rules were used for the interaction between any two different guest molecules. Table SI 13 gives the charges of guest molecules. In Table SI 12 and Table SI 13, these parameters were directly taken from TraPPE force field.[26]

Table SI 4: Pairwise parameters for the interactions between CO_2 and framework (Mg-MOF-74) atoms.

Pairwise interactions		Force field parameters			
Framework	Molecule	$A*10^7$ (K)	B ($Å^{-1}$)	$C*10^5$ ($KÅ^{-5}$)	$D*10^5$ ($KÅ^{-6}$)
Mg	$O(CO_2)$	4.067	4.152	0	4.062
O_a	$O(CO_2)$	1.401	3.330	0.636	0
O_b	$O(CO_2)$	1.673	3.520	0	0.891
O_c	$O(CO_2)$	1.468	3.399	1.160	0
C_a	$O(CO_2)$	2.280	4.065	1.445	0
C_b	$O(CO_2)$	1.408	3.348	0	0.907
C_c	$O(CO_2)$	2.139	3.786	1.194	0
C_d	$O(CO_2)$	0.562	3.006	0	1.756
H	$O(CO_2)$	2.153	4.180	0	0.824
Mg	$C(CO_2)$	7.395	4.770	0	0
O_a	$C(CO_2)$	23.047	4.990	0	0
O_b	$C(CO_2)$	23.047	4.990	0	0
O_c	$C(CO_2)$	23.047	4.990	0	0
C_a	$C(CO_2)$	6.900	4.190	0	0
C_b	$C(CO_2)$	6.900	4.190	0	0
C_c	$C(CO_2)$	6.900	4.190	0	0
C_d	$C(CO_2)$	4.584	4.050	0	0
H	$C(CO_2)$	6.261	5.000	0	0

Table SI 5: Pairwise parameters for the interactions between CO_2 and framework (Zn-MOF-74) atoms.

Pairwise interactions		Force field parameters			
Framework	Molecule	$A*10^7$ (K)	B ($Å^{-1}$)	$C*10^5$ ($KÅ^{-5}$)	$D*10^5$ ($KÅ^{-6}$)
Zn	$O(CO_2)$	1.831	3.675	0	3.946
Zn	$C(CO_2)$	8.205	5.000	0	0

Table SI 6: Pairwise parameters for the interactions between CO_2 and framework (MOF-5) atoms.

Pairwise interactions		Force field parameters			
Framework	Molecule	$A*10^7$ (K)	B ($Å^{-1}$)	$C*10^5$ ($KÅ^{-5}$)	$D*10^5$ ($KÅ^{-6}$)
Zn	$O(CO_2)$	24.53	5.000	0	1.228
O_{ab}	$O(CO_2)$	1.957	3.600	1.052	0.018
O_{cent}	$O(CO_2)$	5.121	4.040	0	1.684
C_a	$O(CO_2)$	0.752	3.291	0	1.767
C_b	$O(CO_2)$	1.771	3.527	0.403	1.742
C_d	$O(CO_2)$	0.726	3.167	0	1.441
H	$O(CO_2)$	2.153	4.180	0	0.824
Zn	$C(CO_2)$	8.205	5.000	0	0
O_{ab}	$C(CO_2)$	23.047	4.990	0	0
O_{cent}	$C(CO_2)$	23.047	4.990	0	0
C_a	$C(CO_2)$	6.900	4.190	0	0
C_b	$C(CO_2)$	6.900	4.190	0	0
C_d	$C(CO_2)$	4.584	4.050	0	0
H	$C(CO_2)$	6.261	5.000	0	0

Table SI 7: Pairwise parameters for the interactions between N_2 and framework (Mg-MOF-74) atoms.

Pairwise interactions		Force field parameters			
Framework	Molecule	$A*10^7$ (K)	B ($Å^{-1}$)	$C*10^5$ ($KÅ^{-5}$)	$D*10^5$ ($KÅ^{-6}$)
Mg	$N(N_2)$	13.826	4.682	1.166	4.109
O_a	$N(N_2)$	1.183	3.141	0	0
O_b	$N(N_2)$	1.124	3.187	0	0.366
O_c	$N(N_2)$	2.020	3.455	0	1.056
C_a	$N(N_2)$	2.295	4.091	1.256	0
C_b	$N(N_2)$	1.392	3.247	0	0.714
C_c	$N(N_2)$	1.578	3.597	0	1.877
C_d	$N(N_2)$	0.524	2.880	0	2.160
H	$N(N_2)$	2.501	4.180	0	0.729
Mg	$COM(N_2)$	0	0	0	0
O_a	$COM(N_2)$	0	0	0	0
O_b	$COM(N_2)$	0	0	0	0
O_c	$COM(N_2)$	0	0	0	0
C_a	$COM(N_2)$	0	0	0	0
C_b	$COM(N_2)$	0	0	0	0
C_c	$COM(N_2)$	0	0	0	0
C_d	$COM(N_2)$	0	0	0	0
H	$COM(N_2)$	0	0	0	0

*COM = center of mass

Table SI 8: Charges for framework (Mg-MOF-74) atoms.

Atom	Charges (e)
Mg	1.5637
O_a	-0.7654
O_b	-0.7088
O_c	-0.8328
C_a	0.4820
C_b	-0.1354
C_c	0.1890
C_d	-0.1814
H	0.3891

Table SI 9: Charges for framework (Extended Mg-MOF-74) atoms.

Atom	Charges (e)
Mg	1.55271
O_a	-0.77003
O_b	-0.7136
O_c	-0.83773
C_a	0.47603
C_b	-0.15132
C_c	0.20064
C_d	-0.14577
H	0.27731

Table SI 10 Charges for framework (Zn-MOF-74) atoms.

Atom	Charges (e)
Zn	1.4094
O_a	-0.7008
O_b	-0.6681
O_c	-0.7807
C_a	0.4812
C_b	-0.1237
C_c	0.1868
C_d	-0.1690
H	0.3649

Table SI 11: Charges for framework (MOF-5) atoms.

Atom	Charges (e)
Zn	1.3901
O_{ab}	-0.6583
O_{cent}	-1.4000
C_a	0.4681
C_b	-0.0398
C_d	-0.1352
H	0.23265

Table SI 12: Lennard-Jones parameters for guest molecules.

Atom	Lennard-Jones parameters	
	Sigma (Å)	Epsilon (K)
$O(CO_2)$	79.000	3.050
$C(CO_2)$	27.000	2.800
$N(N_2)$	36.000	3.310
$COM(N_2)$	0	0

*COM = center of mass

Table SI 13: Charges for guest molecules.

Atom	Charges (e)
$O(CO_2)$	-0.350
$C(CO_2)$	0.700
$N(N_2)$	-0.482
$COM(N_2)$	0.964

*COM = center of mass

10 Description of the different clusters used in this study

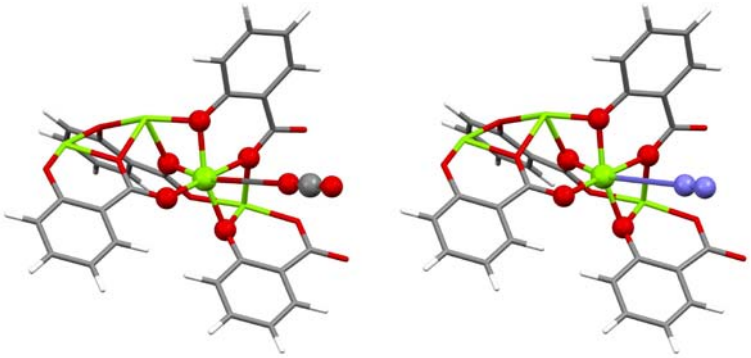

Figure SI 16: (Mg-MOF-74) Mg atom type cluster with CO_2 (left) and N_2 (right) approaching. Color and basis function contraction code: Green (Mg) ball = 17s12p6d2f2g/4s3p1d, Green (Mg) capped stick = 17s12p6d2f2g/3s2p, Red (O) ball = 14s9p4d3f2g /3s2p1d, Red (O) capped stick = 14s9p4d3f2g/2s1p, Gray (C) ball = 14s9p4d3f2g/3s2p1d, Gray (C) capped stick = 14s9p4d3f2g/2s1p, Purple (N) ball = 14s9p4d3f2g /3s2p1d, White (H) capped stick = 8s4p3d1f/1s.

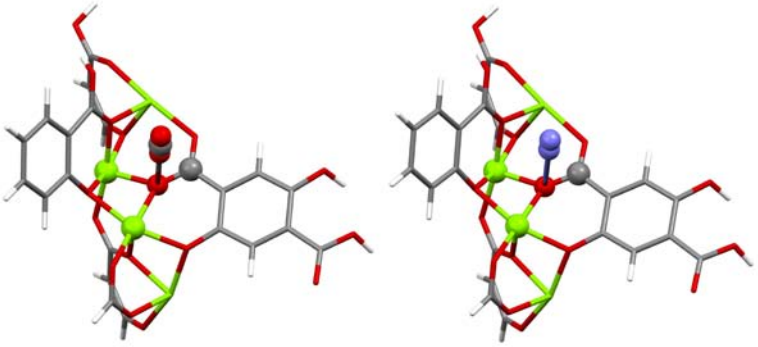

Figure SI 17: (Mg-MOF-74) O_a atom type cluster with CO_2 (left) and N_2 (right) approaching. Color and basis function contraction code: Green (Mg) ball = 17s12p6d2f2g/4s3p1d, Green (Mg) capped stick = 17s12p6d2f2g/3s2p, Red (O) ball = 14s9p4d3f2g /3s2p1d, Red (O) capped stick = 14s9p4d3f2g/2s1p, Gray (C) ball = 14s9p4d3f2g/3s2p1d, Gray (C) capped stick = 14s9p4d3f2g/2s1p, Purple (N) ball = 14s9p4d3f2g /3s2p1d, White (H) capped stick = 8s4p3d1f/1s.

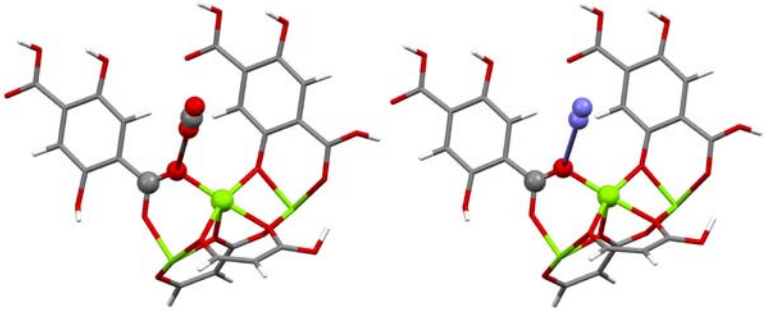

Figure SI 18: (Mg-MOF-74) O_b atom type cluster with CO_2 (left) and N_2 (right) approaching. Color and basis function contraction code: Green (Mg) ball = 17s12p6d2f2g/4s3p1d, Green (Mg) capped stick = 17s12p6d2f2g/3s2p, Red (O) ball = 14s9p4d3f2g /3s2p1d, Red (O) capped stick = 14s9p4d3f2g/2s1p, Gray

(C) ball = 14s9p4d3f2g/3s2p1d, Gray (C) capped stick = 14s9p4d3f2g/2s1p, Purple (N) ball = 14s9p4d3f2g /3s2p1d, White (H) capped stick = 8s4p3d1f/1s.

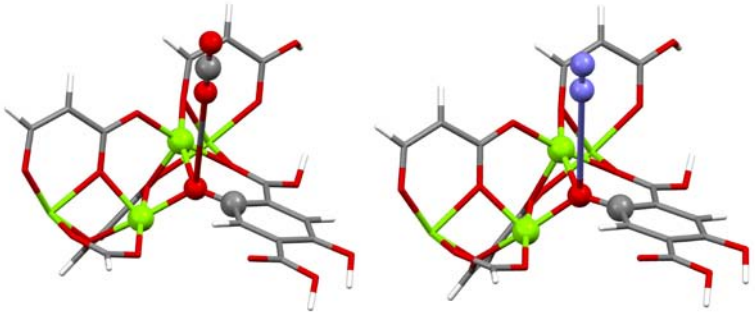

Figure SI 19: (Mg-MOF-74) O_c atom type cluster with CO_2 (left) and N_2 (right) approaching. Color and basis function contraction code: Green (Mg) ball = 17s12p6d2f2g/4s3p1d, Green (Mg) capped stick = 17s12p6d2f2g/3s2p, Red (O) ball = 14s9p4d3f2g /3s2p1d, Red (O) capped stick = 14s9p4d3f2g/2s1p, Gray (C) ball = 14s9p4d3f2g/3s2p1d, Gray (C) capped stick = 14s9p4d3f2g/2s1p, Purple (N) ball = 14s9p4d3f2g /3s2p1d, White (H) capped stick = 8s4p3d1f/1s.

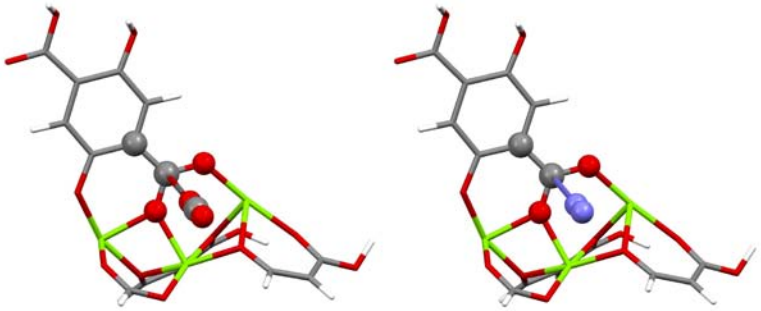

Figure SI 20: (Mg-MOF-74) C_a atom type cluster with CO_2 (left) and N_2 (right) approaching. Color and basis function contraction code: Green (Mg) capped stick = 17s12p6d2f2g/3s2p, Red (O) ball = 14s9p4d3f2g /3s2p1d, Red (O) capped stick = 14s9p4d3f2g/2s1p, Gray (C) ball = 14s9p4d3f2g/3s2p1d, Gray (C) capped stick = 14s9p4d3f2g/2s1p, Purple (N) ball = 14s9p4d3f2g /3s2p1d, White (H) capped stick = 8s4p3d1f/1s.

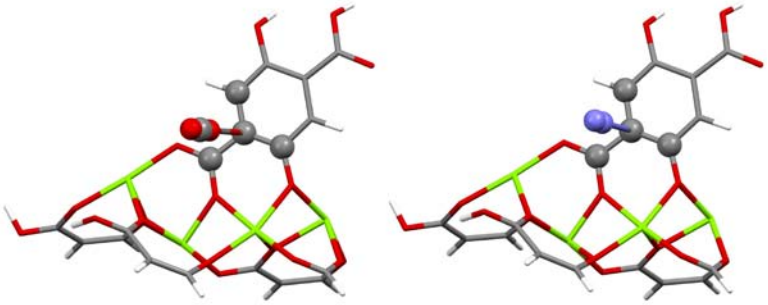

Figure SI 21: (Mg-MOF-74) C_b atom type cluster with CO_2 (left) and N_2 (right) approaching. Color and basis function contraction code: Green (Mg) capped stick = 17s12p6d2f2g/3s2p, Red (O) ball = 14s9p4d3f2g /3s2p1d, Red (O) capped stick = 14s9p4d3f2g/2s1p, Gray (C) ball = 14s9p4d3f2g/3s2p1d, Gray (C) capped stick = 14s9p4d3f2g/2s1p, Purple (N) ball = 14s9p4d3f2g /3s2p1d, White (H) capped stick = 8s4p3d1f/1s.

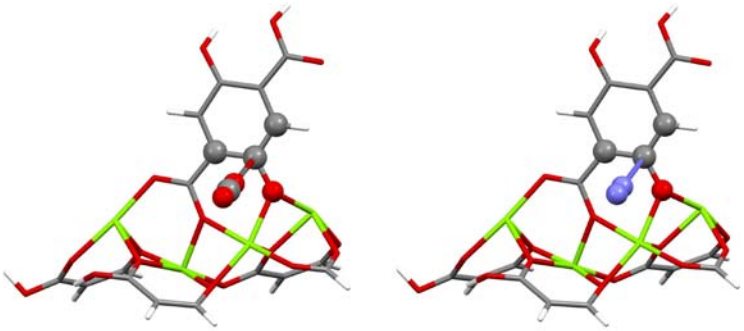

Figure SI 22: (Mg-MOF-74) C_c atom type cluster with CO_2 (left) and N_2 (right) approaching. Color and basis function contraction code: Green (Mg) capped stick = 17s12p6d2f2g/3s2p, Red (O) ball = 14s9p4d3f2g /3s2p1d, Red (O) capped stick = 14s9p4d3f2g/2s1p, Gray (C) ball = 14s9p4d3f2g/3s2p1d, Gray (C) capped stick = 14s9p4d3f2g/2s1p, Purple (N) ball = 14s9p4d3f2g /3s2p1d, White (H) capped stick = 8s4p3d1f/1s.

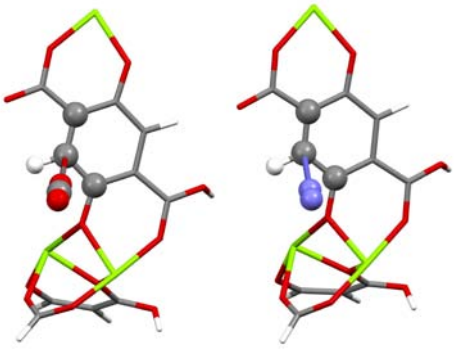

Figure SI 23: (Mg-MOF-74) C_d atom type cluster with CO_2 (left) and N_2 (right) approaching. Color and basis function contraction code: Green (Mg) capped stick = 17s12p6d2f2g/3s2p, Red (O) ball = 14s9p4d3f2g /3s2p1d, Red (O) capped stick = 14s9p4d3f2g/2s1p, Gray (C) ball = 14s9p4d3f2g/3s2p1d, Gray (C) capped stick = 14s9p4d3f2g/2s1p, Purple (N) ball = 14s9p4d3f2g /3s2p1d, White (H) ball = 8s4p3d1f/2s1p, White (H) capped stick = 8s4p3d1f/1s.

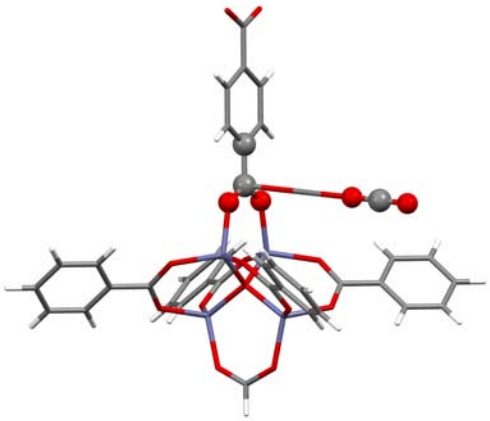

Figure SI 24: (MOF-5) C_a atom type cluster with CO_2 approaching. Color and basis function contraction code: Purple (Zn) capped stick = 21s15p10d6f4g2h/4s3p1d, Red (O) ball = 14s9p4d3f2g /3s2p1d, Red (O) capped stick = 14s9p4d3f2g/2s1p, Gray (C) ball = 14s9p4d3f2g/3s2p1d, Gray (C) capped stick = 14s9p4d3f2g/2s1p, White (H) capped stick = 8s4p3d1f/1s.

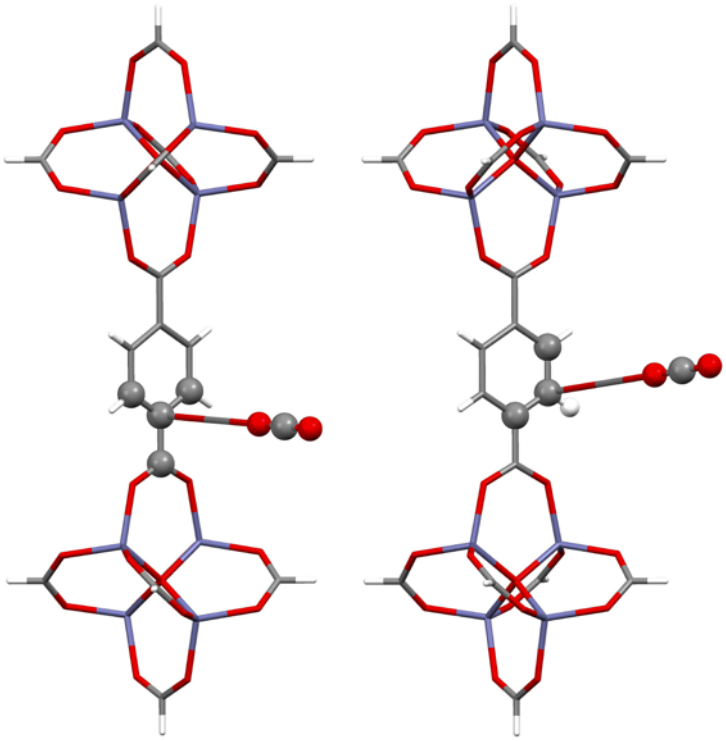

Figure SI 25: (MOF-5) C_b atom type cluster (left) and C_d atom type cluster (right) with CO_2 approaching. Color and basis function contraction code: Purple (Zn) capped stick = 21s15p10d6f4g2h/4s3p1d, Red (O) ball = 14s9p4d3f2g /3s2p1d, Red (O) capped stick = 14s9p4d3f2g/2s1p, Gray (C) ball = 14s9p4d3f2g/3s2p1d, Gray (C) capped stick = 14s9p4d3f2g/2s1p, White (H) ball = 8s4p3d1f/2s1p, White (H) capped stick = 8s4p3d1f/1s.

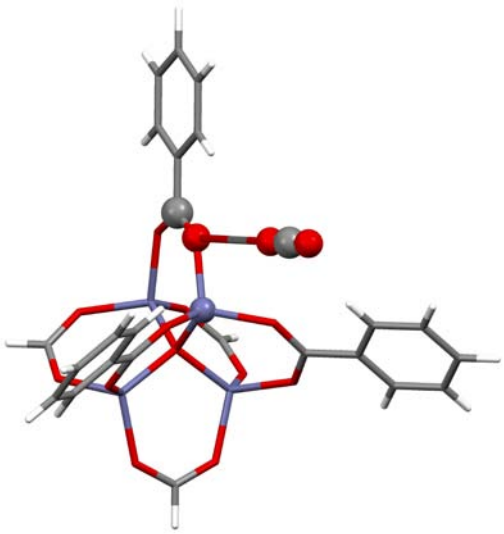

Figure SI 26: (MOF-5) O_{ab} atom type cluster with CO_2 approaching. Color and basis function contraction code: Purple (Zn) ball = 21s15p10d6f4g2h/5s4p2d1f, Purple (Zn) capped stick = 21s15p10d6f4g2h/4s3p1d, Red (O) ball = 14s9p4d3f2g /3s2p1d, Red (O) capped stick = 14s9p4d3f2g/2s1p, Gray (C) ball = 14s9p4d3f2g/3s2p1d, Gray (C) capped stick = 14s9p4d3f2g/2s1p, White (H) capped stick = 8s4p3d1f/1s.

11 Detailed acknowledgements

The research was supported by the U. S. Department of Energy under contracts DE-SC00015, DE-FG02-11ER16283, ARPA-E.

A.L.D. and L.G. were supported by DOE Office of Basic Energy Sciences through project #DE-FG02-11ER16283.

S.N.M, R.P, and B.S. was supported as part of the Center for Gas Separations Relevant to Clean Energy Technologies, an Energy Frontier Research Center funded by the U.S. Department of Energy, Office of Science, Office of Basic Energy Sciences under Award Number DE- SC0001015.

Work at the Molecular Foundry was supported by the Office of Science, Office of Basic Energy Sciences, of the U.S. Department of Energy under Contract No. DE-AC02-05CH11231.

J.A.S. was supported by the Advanced Research Projects Agency - Energy (ARPA-E), U.S. Department of Energy.

L.-C.L. was supported by the Advanced Research Projects Agency - Energy (ARPA-E), U.S. Department of Energy during the initial stage of this project and during the final stage by the Deutsche Forschungsgemeinschaft (DFG, priority program SPP 1570).

J.K. was supported in part by the U.S. Department of Energy under contract DE-AC02-05CH11231 through the Carbon Capture Simulation Initiative (CCSI)

This research used resources of the National Energy Research Scientific Computing Center, which is supported by the Office of Science of the U.S. Department of Energy under Contract No. DE-AC02-05CH11231.

References

1 Boys, S. F. & Bernardi, F. Calculation of Small Molecular Interactions by Differences of Separate Total Energies - Some Procedures with Reduced Errors. *Molecular Physics* **19**, 553-& (1970).

2 Karlstrom, G. *et al.* MOLCAS: a program package for computational chemistry. *Comp Mater Sci* **28**, 222-239, doi:Doi 10.1016/S0927-0256(03)00109-5 (2003).

3 Aquilante, F., Pedersen, T. B. & Lindh, R. Low-cost evaluation of the exchange Fock matrix from Cholesky and density fitting representations of the electron repulsion integrals. *J. Chem. Phys.* **126**, Artn 194106, doi:10.1063/1.2736701 (2007).

4 Aquilante, F., Malmqvist, P. A., Pedersen, T. B., Ghosh, A. & Roos, B. O. Cholesky decomposition-based multiconfiguration second-order perturbation theory (CD-CASPT2): Application to the spin-state energetics of Co-III(diiminato)(NPh). *J. Chem. Theory Comput.* **4**, 694-702, doi:10.1021/Ct700263h (2008).

5 Aquilante, F. *et al.* Accurate ab initio density fitting for multiconfigurational self-consistent field methods. *J. Chem. Phys.* **129**, Artn 024113, doi:10.1063/1.2953696 (2008).

6 Hess, B. A. Relativistic Electronic-Structure Calculations Employing a 2-Component No-Pair Formalism with External-Field Projection Operators. *Phys Rev A* **33**, 3742-3748 (1986).

7 Roos, B. O., Lindh, R., Malmqvist, P. A., Veryazov, V. & Widmark, P. O. Main group atoms and dimers studied with a new relativistic ANO basis set. *J. Phys. Chem. A* **108**, 2851-2858, doi:Doi 10.1021/Jp031064+ (2004).

8 Roos, B. O., Lindh, R., Malmqvist, P. A., Veryazov, V. & Widmark, P. O. New relativistic ANO basis sets for transition metal atoms. *J. Phys. Chem. A* **109**, 6575-6579, doi:Doi 10.1021/Jp0581126 (2005).

9 Rappe, A. K., Casewit, C. J., Colwell, K. S., Goddard, W. A. & Skiff, W. M. UFF, a full periodic table force field for molecular mechanics and molecular dynamics simulations. *J. Am. Chem. Soc.* **114**, 10024-10035, doi:10.1021/ja00051a040 (1992).

10 Gagliardi, L., Lindh, R. & Karlstrom, G. Local properties of quantum chemical systems: The LoProp approach. *J. Chem. Phys.* **121**, 4494-4500, doi:Doi 10.1063/1.1778131 (2004).

11 Holt, A., Bostrom, J., Karlstrom, G. & Lindh, R. A NEMO Potential that Includes the Dipole-Quadrupole and Quadrupole-Quadrupole Polarizability. *J. Comput. Chem.* **31**, 1583-1591, doi:Doi 10.1002/Jcc.21502 (2010).

12 Stone, A. J. *The theory of intermolecular forces*. (Clarendon Press ; Oxford University Press, 1996).

13 Soler, J. M. *et al.* The SIESTA method for ab initio order-N materials simulation. *J. Phys.-Condes. Matter* **14**, 2745-2779 (2002).

14 Kresse, G. & Furthmuller, J. Efficiency of ab-initio total energy calculations for metals and semiconductors using a plane-wave basis set. *Comp Mater Sci* **6**, 15-50 (1996).

15 Kresse, G. & Furthmuller, J. Efficient iterative schemes for ab initio total-energy calculations using a plane-wave basis set. *Physical Review B* **54**, 11169-11186 (1996).

16 Giannozzi, P. *et al.* QUANTUM ESPRESSO: a modular and open-source software project for quantum simulations of materials. *J. Phys.-Condes. Matter* **21**, Artn 395502, doi:10.1088/0953-8984/21/39/395502 (2009).

17 Lee, K., Murray, E. D., Kong, L. Z., Lundqvist, B. I. & Langreth, D. C. Higher-accuracy van der Waals density functional. *Physical Review B* **82**, Artn 081101, doi:10.1103/Physrevb.82.081101 (2010).

18 Roman-Perez, G. & Soler, J. M. Efficient Implementation of a van der Waals Density Functional: Application to Double-Wall Carbon Nanotubes. *Phys. Rev. Lett.* **103**, Artn 096102, doi:10.1103/Physrevlett.103.096102 (2009).

19 Anglada, E., Soler, J. M., Junquera, J. & Artacho, E. Systematic generation of finite-range atomic basis sets for linear-scaling calculations. *Physical Review B* **66**, Artn 205101, doi:10.1103/Physrevb.66.205101 (2002).

20 Moreno, J. & Soler, J. M. Optimal Meshes for Integrals in Real-Space and Reciprocal-Space Unit Cells. *Physical Review B* **45**, 13891-13898 (1992).

21 Queen, W. L. *et al.* Site-Specific CO(2) Adsorption and Zero Thermal Expansion in an An isotropic Pore Network. *J. Phys. Chem. C* **115**, 24915-24919, doi:Doi 10.1021/Jp208529p (2011).

22 Rosi, N. L. *et al.* Rod packings and metal-organic frameworks constructed from rod-shaped secondary building units. *J. Am. Chem. Soc.* **127**, 1504-1518 (2005).

23 Dietzel, P. D. C., Blom, R. & Fjellvag, H. Base-induced formation of two magnesium metal-organic framework compounds with a bifunctional tetratopic ligand. *Eur. J. Inorg. Chem.*, 3624-3632, doi:Doi 10.1002/Ejic.200701284 (2008).

24 Valenzano, L., Civalleri, B., Sillar, K. & Sauer, J. Heats of Adsorption of CO and CO2 in Metal–Organic Frameworks: Quantum Mechanical Study of CPO-27-M (M = Mg, Ni, Zn). *The Journal of Physical Chemistry C* **115**, 21777-21784, doi:10.1021/jp205869k (2011).

25 McDonald, T. M. *et al.* Capture of Carbon Dioxide from Air and Flue Gas in the Alkylamine-Appended Metal–Organic Framework mmen-Mg2(dobpdc). *J. Am. Chem. Soc.* **134**, 7056–7065, doi:10.1021/ja300034j (2012).

26 Potoff, J. J. & Siepmann, J. I. Vapor-liquid equilibria of mixtures containing alkanes, carbon dioxide, and nitrogen. *Aiche J.* **47**, 1676-1682 (2001).

27 Grimme, S. Calculation of the electronic spectra of large molecules. *Rev Comp Ch* **20**, 153-218 (2004).

28 Wu, H., Simmons, J. M., Srinivas, G., Zhou, W. & Yildirim, T. Adsorption Sites and Binding Nature of CO(2) in Prototypical Metal-Organic Frameworks: A Combined Neutron Diffraction and First-Principles Study. *Journal of Physical Chemistry Letters* **1**, 1946-1951, doi:Doi 10.1021/Jz100558r (2010).

29 Caskey, S. R., Wong-Foy, A. G. & Matzger, A. J. Dramatic tuning of carbon dioxide uptake via metal substitution in a coordination polymer with cylindrical pores. *J. Am. Chem. Soc.* **130**, 10870, doi:Doi 10.1021/Ja8036096 (2008).

30 Simmons, J. M., Wu, H., Zhou, W. & Yildirim, T. Carbon capture in metal-organic frameworks-a comparative study. *Energ Environ Sci* **4**, 2177-2185, doi:10.1039/c0ee00700e (2011).

31 Walton, K. S. *et al.* Understanding inflections and steps in carbon dioxide adsorption isotherms in metal-organic frameworks. *J. Am. Chem. Soc.* **130**, 406-407 (2008).

32 Myers, A. L. & Prausnitz, J. M. Thermodynamics of mixed gas adsorption. *American Institute of Chemical Engineers Journal* **11**, 121-130 (1965).